Journal of Interfaces, Thin films, and Low dimensional systems 6 (1) Summer and Autumn (2022) 547-558

Effect of hydrostatic pressure on the Auger recombination rate of InGaN/GaN multiple quantum well laser diode

Scientific research paper

Rajab Yahyazadeh* and Zahra Hashempour

Department of Physics, Khoy Branch, Islamic Azad University, Khoy, Iran

ARTICLE INFO

Article history:
Received 1 March 2023
Revised 15 April 2023
Accepted 6 May 2023
Available online 23 June 2023

Keywords
Auger Recombination
Overlap integrals
Laser diode
Multi-quantum well

ABSTRACT

In this study, a numerical model has been used to analyze the Auger recombination rate in c-plane InGaN/GaN multiple-quantum-well lasers (MQWLD) under hydrostatic pressure. Finite difference techniques are employed to acquire energy eigenvalues and their corresponding eigenfunctions for InGaN/GaN MQWLD. The hole eigenstates are calculated via a 6×6 **k.p** method under the applied hydrostatic pressure. It has been found that a change in pressure up to 10 GPa increases the effective band gap together with the carrier density up to $0.75\times10^{19}\,cm^{-3}$ and $0.56\times10^{19}\,cm^{-3}$ for the holes and electrons, respectively. Based on the results, it could decrease the exaction binding energy, rise the electric field rate up to $0.77\,MV/cm$, and decrease the Auger recombination rate down to $0.6\times10^{17}\,cm^{-3}s^{-1}$ in the multiple-quantum well regions. Also, calculations demonstrate that the hole-hole-electron (CHHS) and electron-electron-hole (CCCH) Auger recombination rate has the largest contribution towards the Auger recombination rate. Our studies provide more detailed insight into the origin of the Auger recombination rate drop under hydrostatic pressure in InGaN-based LEDs.

1 Introduction

Non-radiative recombination is performed in the form of deep and shallow traps, interface roughness, and defects, as well as band-to-band and phonon-assisted Auger recombination (BBAR & PAAR) [1-5]. The Auger recombination is one of the most important mechanisms in reducing the efficiency of photovoltaic devices [6-8]. BBAR is one of the essential non-radiative recombination techniques that has attracted the attention of different researchers in the field of InGaN/GaN photovoltaic devices [9-11]. Auger recombination is the most important parameter to obtain Auger coefficient and Auger current. Various numerical and analytical models have been used to calculate the Auger and lifetime recombination. Picozzi et al. studied the lifetime of this Auger through the first-principle detail balance based on the density function method at different carrier concentrations in semiconductors [12]. Likewise, Anatoli et al. evaluated the effect of temperature and well width on the Auger recombination using the Khans model in a semiconductor quantum well [13]. In addition, Piperk et al. investigated the dependence of the Auger coefficient on the carrier density, band gap, and wavelength through the ABC model on gallium *nitride* (GaN)- and nitride-based light-emitting diodes (LEDs) [7, 14]. McMahan et al. also focused on the atomistic analysis of Auger recombination in InGaN/GaN quantum wells under temperature [15]. Non-radiative Auger recombination generates a non-radiative current in photovoltaic devices such as solar cells, lasers, and diodes. Therefore, it is necessary to carefully study the dependence of all parameters effective in this

*Corresponding author.
Email address: Rajab.yahyazadeh@iaukhoy.ac.ir
DOI: 10.22051/jitl.2023.43080.1082

recombination under external perturbations such as hydrostatic pressure or temperature. In this regard, the most important parameters are carrier density, effective band gap energy, carrier energy (from the band structure) built-in polarization field, carrier localization length, and overlap integral of wave functions. In this paper, changes in all the above-mentioned parameters are calculated and investigated under hydrostatic pressure in InGaN/GaN multiple-quantum well light-emitting diodes. The Auger recombination rate is one of the most essential parameters in calculating the Auger coefficient and the Auger current of laser diodes. Thus, careful study of the Auger current requires precise investigation of the Auger recombination rate which is the main purpose of this paper under hydrostatic pressure. The use of five vital parameters, including effective mass, energy gap, lattice constants, dielectric constant and quantum barrier, and well thickness, is the most significant advantage of this numerical method and the innovation of this work besides the fact that all the mentioned parameters simultaneously depend on hydrostatic pressure and temperature. This study has also addressed the effect of hydrostatic pressure on the energy of heavy, light, and split-off band holes. In this model, the conduction band energy, wave functions, Fermi level, and energy subbands are obtained from the self-consistent solution of the Schrödinger and Poisson equations. The current study has also considered the effective width of the quantum wells, which depends on the carrier density, which is not constant. It should be noted that the Femi level has also been computed using another method that enables convergence in a sophisticated way [16]. The hole valence band (heavy, light, and split-off band holes) energy, wave functions, and energy subbands are calculated using a 6×6 **k.p** method.

2 Calculations and model

The quantum-well laser diodes (QWLD) consist of a multiple-quantum-well structure in the intrinsic region of a p–i–n. The MQW structure introduced for the model is constructed by $In_mGa_{1-m}N$ with lower indium molar fraction (m=0.4) for barriers and m=0.5 for wells (Fig. 1). The sample used in the modeling is the p–i–n light-emitting diodes with an InGaN/GaN MQWSC structure within the i-region. The p and n regions are based on GaN. The donor and acceptor concentrations in the n- and p-region materials are assumed to be the same equal to $0.1\times10^{18}\,cm^{-3}$ while 10 wells are considered in the current work. In addition, atmospheric and hydrostatic pressures are taken into account (i.e., at zero hydrostatic pressure), but only the atmospheric pressure is applied for evaluation. Both Schrödinger and Poisson equations must be solved to obtain accurate values for the Fermi energy, the energies of quantized levels within the two-dimensional electron gas (2DEG), potential profiles, wave function, and the sheet carrier concentration for 2DEG in InGaN/GaN heterostructures. This is achieved by solving Schrödinger's equation and simultaneously taking into account the electrostatic potential obtained from Poisson's equation, as well as the image and exchange-correlation potentials using the three-point finite difference method [17]. In the Schrödinger equation, built-in potential energy is considered, which is the potential energy induced by spontaneous (SP) and piezoelectric (PZ) polarization charges [18-20]. In this work, five parameters are used, namely, effective mass, energy gap, lattice constants, dielectric constant and quantum barrier, and well thickness, which simultaneously rely on hydrostatic pressure and temperature. The basal strain $\grave{o}(T,P,m)=\left(a_s-a_e(T,P,m)\right)/a_e(T,P,m)$ is expressed from the lattice of the substrate a_s and the epilayer $a_e(T,P,m)=a_0(m)\left[\left(1+\beta\left(T-T_{ref}\right)\right)\left(1-P/3B_0\right)\right]$ [21,22]. The lattice constants are the functions of temperature, indium molar fraction, and the hydrostatic pressure, where $B_0=239GPa$ is the bulk modulus of sapphire. Further, $\beta_{GaN}=5.56\times10^{-6}K^{-1}$ and $T_{ref}=300K$. $a_0(m)=0.13989m+0.03862$ represents the thermal expansion coefficient and the equilibrium lattice constant as a function of indium molar fraction, respectively [21-23]. Here, the dielectric constant and the thickness of InGaN/GaN depend on the hydrostatic pressure and temperature [23]. In our strained InGaN/GaN quantum wells, the conduction bands are assumed to be parabolic. This is while nonparabolic valence bands are computed by a 6 x 6 **k.p** method [24-27].

To calculate the BBAR rate in InGaN/GaN MQWs, we broadly follow the method presented prior to the present study [27]. We will only focus on the CHHS (one electron ($1'$) and two heavy holes ($1,2$) and one split of band hole ($2'$)) Auger process because CHHL (one

electron, two heavy holes, and light hole) and CCCH (three electrons and one heavy hole) processes can be derived by a similar way. Auger processes involving phonons are generally not important for relative consideration at room temperature; here as a result, only three BBARs are considered in this study [28]. From Fermis's Golden Rule, the Auger transition rate per unit volume for the CHHS process in quantum well is given by [29]:

$$R_A = \frac{1}{4\pi\hbar L_{eff}}\left(\frac{e^2}{4\pi\varepsilon_w}\right)^2\left(\frac{4\pi}{(2\pi)^3}\right)^2 \times \sum_{allE_z}\int\int\int\int \overbrace{|\mathrm{k}\text{-}\mathrm{k}'|^{-2}A_k^2}^{M}\,\delta(k_1\text{-}\mathrm{k}_{1'}+\mathrm{k}_2\text{-}\mathrm{k}_{2'})P_{1,1',2,2'}\delta(E)d^2k_1d^2k_{1'}d^2k_2d^2k_{2'}, \quad (1)$$

where $L_{eff} = (1/n)\int_0^{L_{InGaN}} zn(z)dz$ represents the effective width of the 2DEG channel [30]. Further, $n(z)$ and ε_w denote the quantum well sheet density along the growth direction (z-direction) and the dielectric constant of the InGaN, respectively. Furthermore, $\delta(E)$ expresses the energy conservation between initial (particles $1,2$) and final ($1',2'$) states, M is the matrix element of Coulomb interaction potential between two holes,while A_k is the overlap integral. Moreover, $P_{1,1',2,2'} \approx f_{v1}f_{c1'}f_{v2}[1-f_{v2'}]$ accounts for the sate occupations. The approximation is employed considering that the excited carrier has extremely high energy. Additionally, $f_c = \frac{1}{\left(1+\exp\left(\frac{E_c-E_{fc}}{k_bT}\right)\right)}$ and $f_v = \frac{1}{\left(1+\exp\left(\frac{E_v-E_{fv}}{k_bT}\right)\right)}$ are the Fermi-Dirac distribution for the electrons of conduction bands and holes in valence bands, respectively, where E_c and E_v are the quantized electron and hole energy levels, respectively. In addition, E_{f_c} and E_{f_v} represent the electron and hole quasi-Fermi levels, respectively. In relation 1, all the energies of the allowed transitions related to the subbands of the carriers are considered in the z-direction, following the selection rule. A detailed study of the effect of pressure on Auger recombination requires a detailed study of each of these parameters. The relation of the overlap integral in the Auger recombination is as follows [29]:

$$\boldsymbol{A_k = F_{11'}F_{22'}\times \iint dz_1dz_2\phi_1(z_1)\,\phi_{1'}(z_1)\phi_2(z_2)\phi_{2'}(z_2) \times \exp(-|k_1-k_{1'}|.|z_1-z_2|) = I_{11'}(|k_1-k_{1'}|)I_{22'}(-|k_1-k_{1'}|),} \quad (2)$$

where the particle state in the quantum well is represented by the product of a localized Bloch wave function, a plain wave term, and a confined-state wave function (ϕ). Further, k and $k_{1'}$ are the 2D wave vectors in the plain of the well carrier $\{1,1'\}$, respectively. At the beginning of each of the recombination stages (CHHS, CCCH, & CHHL), first, the electron and the hole must be recombined $(1,1')$ until the second stage $(2,2')$. In relation A_k, the integral contribution of the electron and hole overlap, $I_{eh} = I_{11'} = F_{11'}\int dz_1\phi_1(z_1)\phi_{1'}(z_1)e^{-|k_1-k_{1'}|.z_1}$, is the most important parameter to start the recombination. Furthermore, $I_{11'}$ denotes the overlap integral between the localized (the subband state in quantum wells) states. Moreover,

$$I_{22'}(-|\boldsymbol{k}-\boldsymbol{k'}|) = I_{hx} = F_{22'}\int dz_2\phi_2(z_2)\phi_{2'}(z_2)e^{-|k_I-k_I|.z_2}$$

indicates the overlap integral between the localized and excited (electron or hole) states. The excited states of particle $2'$ may be bound (subband) or unbound (even or odd) [28]. In this case, the contribution of each of these bound and unbound states in the Auger recombination will be R_A^b, R_A^e, and R_A^o, respectively [29], where b, e, and o represent bound, even, and odd, respectively. The overlap function of the electron and hole is non-linear with respect to $|k_1-k_{1'}|$. Additionally, $F_{11'} = \frac{(\alpha_{CH}|k_1-k_{1'}|)}{E_g}$ and $F_{22'} = \frac{(\alpha_{SH}|k_1-k_{1'}|)}{E_g}$ are the overlap integral of the localized Bloch function between carrier $\{1,1'\}$ and $\{2,2'\}$, respectively. $\alpha_{SH} = -(\hbar^2/4m_0)\{[(m_0/m_l)+(m_0/m_H)+(m_0/m_S)-3]\}$ and $\alpha_{CH} = (\hbar^2/4m_0)[(m/m_c)-1]$ are the overlap parameter. In addition, the value of $|k_1-k_{1'}|$used in $F_{11'}$, $F_{22'}$, and A_k for the CHHS Auger process is as follows:

$$\left|k_1 - k_{1'}\right|^2 = \frac{\left[2m_s(m_h + m_e)^2\left(E^{eff} - \Delta_{S0}\right)\right]}{\left[\hbar^2(2m_h + m_e - m_s)(2m_h - m_e)\right]}. \quad (3)$$

$\left|k_1 - k_{1'}\right|$ depends on parameters such as effective band gap (E_{eff}), the spin-orbit splitting (Δ_{so}), electron $\left(m_e^*\right)$, heavy hole $\left(m_h^*\right)$, and the split-off band $\left(m_s^*\right)$ effective mass, respectively.

The effective band gap relation is written as [29,31,32]:

$$E_{eff} = \overbrace{E_g^{InGaN} + E_1^e + E_{1'}^{hh} - E_b^{e,hh} - eF_W L_{eff}}^{E_{11'}^{e,hh}} + E_2^{hh} - E_{2'}^{so}, \quad (4)$$

where $E_{11'}^{e,hh}$ is the transition energy of the electron from the conduction band to the heavy hole in the valence band, while E_1^e, $E_{1'}^{hh}$, and E_2^{hh} are the bond state energy along the z-direction. In addition, $E_{2'}^{so}$ is the excited carrier energy along the z-direction which can be either bound or unbound. Further, $E_b^{e,hh}$ denotes the bounding energy of exciton, which depends on external perturbation such as pressure and temperature through electron and hole effective masses [32-34]. Exciton energies are determined by employing a variational procedure [35-38].

Furthermore, $E_g(T,P) = E_g(0,0) + \gamma P + \sigma P^2 + \left(\alpha T^2\right)/\left(T + T_e\right)$ is the band gap energy of InGaN/GaN [19,21,23], while $E_g(0,0)$ stands for the band gap energy of GaN or InGaN in the absence of the hydrostatic pressure and at temperature 0K. In this work, the parameters α, σ, and γ are independent of the electron concentration, whose numerical values are listed in Table 1. Moreover, F_w represents the electric field in the well caused by polarization charges. In calculating the band gap energy and SP polarization that rely on indium molar fraction (m), indium molar fraction was considered independent of the location (along the well and barrier). To investigate external perturbation such as pressure and the effect of the overlap integral, which has a direct relationship with the quantum confinement, the wave functions of the first subband of the carriers (ψ) were considered to calculate the localization length in the z axis as $(\Delta z) = \int \left|(z - \langle z \rangle)\psi\right|^2 dz$, where $\langle z \rangle = \int z\left|\psi\right|^2 dz$ [39]. The limits of the integral are taken into account from the center of the neighboring barrier adjacent to the center of the quantum well. The electron density in the quantum well is written as [40]:

$$n_w(z) = \sum_{i=1}^{5} \frac{(m_e^* K_B T)}{\pi\hbar^2} Ln\left[1 + exp\left(\frac{E_F - E_i}{K_B T}\right)\right] \psi_i^2(z), \quad (5)$$

where K_B, E_F, i, ψ_i, and T denote the Boltzmann constant, Fermi level, subband level index, electron wave function in the i-th subband, and absolute temperature, respectively [36]. m^* is an average electron effective mass in the $k_x - k_y$ plane so that it can be written as in conduction band edge as follows [35]:

$$\frac{m_0}{m_e^*(P,T,m)} = 1 + \frac{\left[E_P^\Gamma\left(E_g^\Gamma(P,T,m) + 2\Delta_{S0}/3\right)\right]}{E_g^\Gamma\left(E_g^\Gamma(P,T,m) + \Delta_{S0}\right)}, \quad (6)$$

where m_0, E_P^Γ, and Δ_{S0} are the free electron mass, the energy linked to the momentum matrix element, and the spin-orbit splitting, respectively, whose numerical values are listed in Table 1. The hole wave functions and energy subbands are calculated along the Z axis using a 6×6 **k.p** method [24-27,41]. The hole distribution is computed by summing contributions from five hole subbands. A formulation is used to determine the hole distribution as follows [42]:

$$p_w(z) = \left(\frac{m_h^* K_B T}{\pi\hbar^2}\right) \sum_{i=1}^{5} \sum_{\upsilon}^{3} \mathrm{Ln}\left[1 + exp\left(\frac{E_F - E_i}{K_B T}\right)\right] \left|g_i^\upsilon(z)\right|, \quad (7)$$

where m_h^* and E_i represent an average hole mass in the $k_x - k_y$ plane and the hole eigenvalue, respectively. Additionally, $g_i^\upsilon(z)$ is the envelope function associated with the n-th basis state of the Hamiltonian. Further, the summation over n and i are over the three basis states and the hole wave functions, respectively. The envelope functions are normalized such that $\sum_{\upsilon=1}^{3} \int_0^{L_{GaN}} \left|g_i^\upsilon(z)\right|^2 dz = 1$.

To calculate effective masses depending on the threshold energy (the minimum energy for the split-off hole in the CHHS Auger process), it is necessary to use the band structure obtained from the **k.p** model and the following relationship [29,43,44]:

$$E_T = \left[\frac{(2m_H + m_C)}{(2m_H + m_C - m_S(E_T))}\right](E_{eff} - \Delta_{S0}). \quad (8)$$

This relationship is for the case where the effective band gap is greater than Δ_{S0} [44]. For the case where the effective band gap is less than Δ_{S0}, the threshold energy is exactly equal to Δ_{S0}. The effective mass at the threshold voltage is obtained through the self-consistent solution. In the threshold energy, m_S relies on the threshold voltage. Furthermore, convergence is obtained when the difference in the threshold energy associated with two consecutive iterations $(E_{T(n)} - E_{T(n-1)})$ is smaller than $10^{-4} eV$. The threshold voltages of the Auger recombination of CCCH and CHHL is the same as equation CHHS, except that the effective masses of the electron ($m_C(E_T)$) and light hole ($m_L(E_T)$) will depend on the threshold voltage, respectively, and they are Δ_{S0} times zero. The effective mass of the carriers in each of the subbands of the quantum wells (electrons and holes) can be calculated after determining the effective mass of the carriers in the GaN barrier and the InGaN/GaN well. The carrier effective mass in the i-th subband, $1/m_i^* = (1/m_b^*)[1 - P_{iw}] + P_{iw}/m_w^*$, can be computed [39,29], where m_b^* and m_w^* are the barrier and well carrier effective masses, and $P_{iw} = P_{iw}(\psi_{iw}) / \left(P_{ib}(\psi_{ib}) + P_{iw}(\psi_{iw})\right)$ is the probability of finding an electron in the quantum well at the level with energy E_i. Moreover, $P_{iw}(\psi_{iw}) = \int_0^{L_{GaN}} dz |\psi_{iw}|^2$ and $P_{ib}(\psi_{ib}) = \int_{-L_{InGaN}}^{0} dz |\psi_{ib}|^2$ are the wave function of the electron in the i-th subband and the wave function penetrating toward the quantum barrier, respectively. The value of the penetrating wave function in the barrier $\left(P_{ib}(\psi_{ib})\right)$ is the criterion for determining the quantum confinement that is effective in the effective masses of the carriers in subbands. As mentioned earlier, the effective masses of light and heavy holes are obtained using the 6×6 **k.p** method [25,26]. Binary effective mass parameters are linearly interpolated to obtain InGaN values. The numerical values of the valance band effective mass parameters (Ai) and deformation potentials (Di) have been extracted from reference [46]. The effective masses in $m^*_{In_xGa_{1-x}N}$ barriers can be obtained by determining the effective masses of carriers in quantum wells through the ternary formula $1/m^*_{In_xGa_{1-x}N} = \left((1-x)/m^*_{InN}\right) + x/m^*_{GaN}$ [47]. Finally, the Auger recombination is defined as [29]:

$$R_A(InGaN) = R_A(CHHS) + R_A(CHHL) + R_A(CCCH). \quad (9)$$

The 2D Auger recombination rate and coefficient can be translated into common 3D rates using the quantum well thickness, which are $R_A = R_{2D} / L_{eff}$ and $C_A = L_{eff}^2 C_{2D}$ [9].

3 Results and discussion

In this paper, a numerical model was presented to calculate the optical parameters of *InGaN / GaN* multiple-quantum-well light-emitting diodes (MQWLED) and investigate the effect of hydrostatic pressure. In addition, Schrödinger's and Poisson's differential equations were solved by the finite difference method. However, the iterative method [17,50] was used in the step of the self-consistent solution of Schrödinger-Poisson equations. The convergence is obtained when the difference on the Fermi level is associated with two consecutive iterations $(E_{F(n)} - E_{F(n-1)})$ and is smaller than $10^{-4} eV$. During the calculations, the same grid mesh was also employed for both Poisson and Schrödinger equations. The hole eigenstates were computed using a 6×6 **k.p** method. Conduction and valance bands with the location of quantum wells (electrons and holes), as well as valance bands for light, heavy, and split-off band holes, are shown in Fig. 1. To evaluate parameters related to the LED and start Auger recombination, a positive voltage of 1.5 V was applied to region p-GaN. In this case, the multi-quantum wells of electrons and holes are below the Fermi level (Fig. 1).

Figure 2 illustrates an example of a change in an electron quantum well in position -50 nm to carefully study changes in the quantum well. As depicted in the inset of Fig. 2, increasing the hydrostatic pressure in the range of 0-10 GPa has led to an increase of up to 65

meV and $1.8\times10^{17}m^{-2}$ in the quantum well depth and interface polarization charge density (σ_b), respectively. This phenomenon is related to the correction of the atomic distances of the crystal lattice by external pressure, which also leads to a change in polarization. As the pressure increases, σ_b rises due to the increase in PZ polarization and spontaneity. Likewise, the lattice constants ($a_e(T,P,m), a_0(m)$) increase with an increase in hydrostatic pressure.

According to Fig. 3, an increase in polarization causes increases the internal electric field and the total electric field, causing the centers of positive (holes) and negative (electrons) charges to move away from each other. For the pressure from 0 to 10 GPa, the electric field changes in the multiple-quantum well are $0.77MV/cm$. Further, the hole quantum well in position 150 nm and the electron quantum well in position -50 nm are $6.1MV/cm$ and $3.2MV/cm$, respectively. An increase in the electric field and quantum well depth causes an increase in carrier density (Figs. 4 and 5). By increasing pressure by 10 GPa, the density of holes and electrons increases and carriers in quantum wells (position -50 and 150 nm) are injected into the region of multiple-quantum wells, affecting the Auger recombination. The density increase in the region of the multiple-quantum well (and for example, in the position of the fifth well) is $0.56\times10^{19}cm^{-3}$ and $0.75\times10^{19}cm^{-3}$ for electrons and holes, respectively. The changes in carrier density in the fifth well are depicted in Figs. 4 and 5.

To determine the dependence on the pressure of the effective mass through Eq. (8), it is necessary to calculate the transition energy, exciton binding energy, and effective band gap. Figure 7 displays the dependence of the transition energy on the pressure after determining the internal field, the energy of the subbands, and the energy of the exciton binding energy. Based on the results, the transition energy and effective band gap of the first subband of the carriers (with the highest density) are plotted to investigate the hydrostatic pressure effect. The obtained data revealed that the transition energy and effective band gap increase with an increase in pressure, the main factor which is the increase in surface and carrier densities. The binding energy of excitons as a function of hydrostatic pressure is illustrated in the inset of Fig. 6. As shown, the decrease in the exciton binding energy with increasing pressure can be explained by the internal electric fields. With increasing pressure, SP and PZ polarization increases, thereby increasing the internal electric fields. The electric fields separate the electron and holes in the opposite direction, expanding the distance between electrons and the holes, thus reducing the Coulomb interaction.

In determining Auger recombination, effective masses play the most important role, and we must know the dependence on external perturbation such as hydrostatic pressure. This work requires the calculation of the band structure of valence carriers; this process for quantum well InGaN/GaN is shown in Fig. 7. In the direction of the in-plain wave vector (kx or ky), all bands are non-parabolic energy. Heavy holes are independent of pressure, and the slope of the graph is almost constant with the change of pressure, indicating that the effective mass of heavy holes remains unchanged with the increase of the wave vector and pressure. However, light and split-off holes, as well as their effective masses (the radius of curvature), change with increasing pressure so that the effective mass of light holes almost approaches heavy holes after the wave vector of 1.03 nm^{-1}. These mass changes with pressure and wave vector are effective in computing the threshold voltage. According to Fig. 7, an increase in the pressure of 10 Gpa (at the band edge k=0) causes a change in the energy of 42, 48, and 290 meV for heavy, light, and split-off holes, respectively. The effective mass of split-off holes is lower than that of light holes, and they tend to receive energy from electron-hole recombination in Auger recombination. Therefore, the non-radiative recombination of CHHS is expected to be higher than that of CHHL for the InGaN/GaN quantum well. By specifying the band structure, the transition energy and effective masses can be calculated.

The overlap integral can be determined after determining the effective masses of carriers and transition energy. In the overlap integral A_k, there is an overlap of electron and hole I_{eh}, in all recombination process, and here, the overlap of the wave functions (the first subband of electrons and heavy holes) versus the transfer momentum $(k_{11'}=k_1-k_{1'})$ is checked at different pressures (Fig. 8). Based on the results, increasing the pressure reduces the overlap of electron and hole wave functions. According to Fig. 8, the overlap is a non-linear function depending on the size of the transfer momentum. In the small transfer

momentum, the overlap and recombination are reduced so that the hydrostatic pressure will have a reduced role in the recombination. The effect of hydrostatic pressure on the transfer momentum near the origin (non-resonant) is small. In the resonance mode $(k_{11'} = k_1 - k_{1'})$, the energy of the transition $(\hbar^2 k_{11'}^2/(2m_c) = E_{11'}^{e,hh})$ becomes the same as the energy between heavy and split-off holes in the direct transition. The overlap of wave functions is one of the most important parameters in Auger recombination. The overlap integral also depends on the overlap integral I_{hx} between the localized and excited (electron and hole) states. To compare both overlap integrals, we plot their overlap in the positive part of $k_{11'}$. From a mathematical point of view, I_{hx} is an integral between the smooth wave function of a carrier localized in the quantum well (with wave vector $k_{11'} \square \pi / L_{eff}$) and the highly oscillating wave function of an excited carrier (with wave vector $k_{11'} \square k_g$). As a consequence, the overlap integral I_{hx} is normally small compared to I_{eh}. As shown, the contribution of 85% of the total overlap integral is related to I_{eh}, which is under the pressure of the maximum change. To more precisely investigate the effect of pressure on the carrier overlap, we draw the first subband wave functions for the quantum well (at position 45-50 nm, Fig. 9), and then obtain the localization length (Fig. 10). According to Fig. 10, the wave functions of heavy holes are more localized than all carriers, while those of electrons and split-off holes are delocalized. By plotting the localization length based on Fig. 10, with increasing pressure by 10 GPa, the localization length of heavy holes and electrons decrease by 1 and 3.8 nm, respectively. The least impact of pressure is on heavy holes, and for this reason, unlike electrons which are affected by pressure, heavy holes can participate more in the CHHS Auger process. As a result, by increasing pressure by 10 GPa, the depth of the quantum well, the quantum confinement of the carriers, and the localized length of all carriers are greater. The contribution of each of the recombination rate is shown in Fig. 11, the highest of which is related to $R_A(CHHS)$. The reason for this is related to the localization length of heavy holes, which was explained earlier. Finally, the overall recombination rate decreases with increasing pressure (Fig. 12).

Tablel 1. Suggested Parameters for GaN and InN

Parameters(unit)	GaN	InN	References
E_P^{Γ}(eV)	14.0	14.5	[46]
E_g^{Γ}(0K=0GPa)(eV)	3.42	0.7	[46]
Δ_{s0}(eV)	0.014	-0.001	[46]
γ(meV.GPa^{-1})	31.8	16	[22]
δ(meV.GPa^{-2})	-0.23	-0.02	[22]
S_{11}(10^{-2}GPa)	0.55	1.15	[19]
S_{12}(10^{-2}GPa)	0.19	0.46	[19]
α(10^{-3}eV.K^{-1})	0.909	0.245	[46]
T_e(K)	830	624	[46]
ε_∞	5.39	6.7	[51]

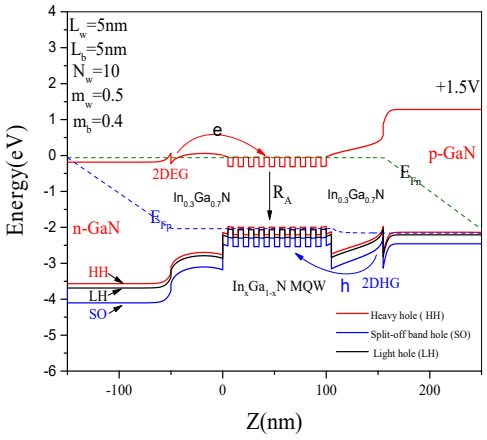

Figure 1. The conduction (C.B) and valence (V.B) band energy of InGaN/GaN MQW light-emitting diode as a function of the distance under different hydrostatic pressure.

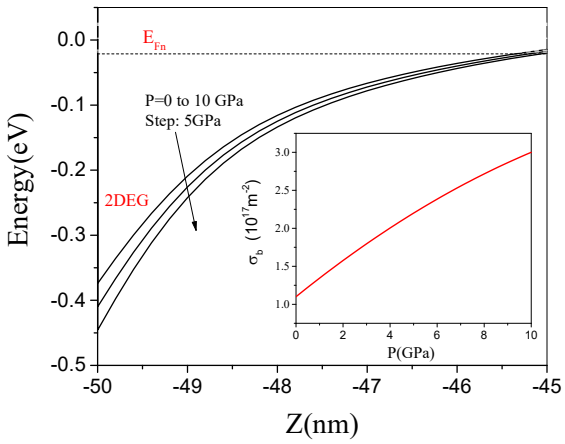

Figure 2. The quantum-well conduction band energy as a function of the distance under different hydrostatic pressures**.** The inset indicates the variation of InGaN/GaN interface polarization charge density (σ_b) as a function of the hydrostatic pressure.

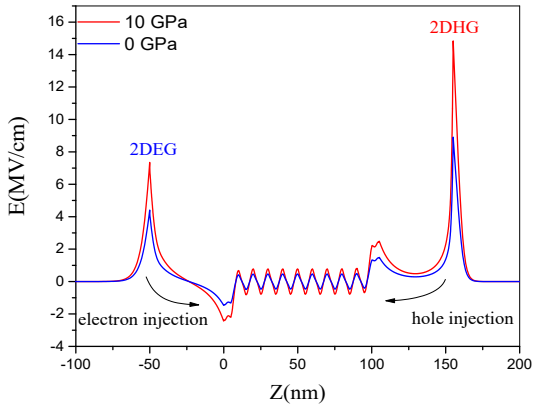

Figure 3. Electric field of InGaN/GaN MQW light-emitting diode as a function of the distance under different hydrostatic pressure.

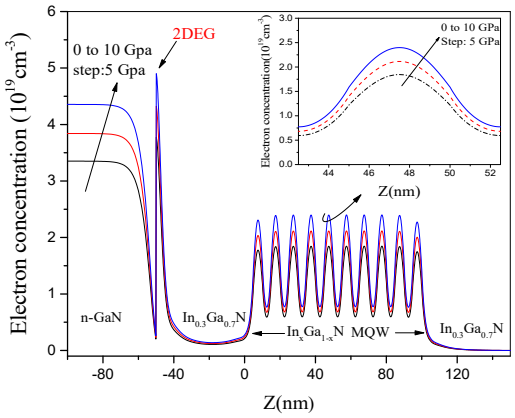

Figure 4. Electron concentration of InGaN/GaN MQW light-emitting diode as a function of the distance under different hydrostatic pressure.

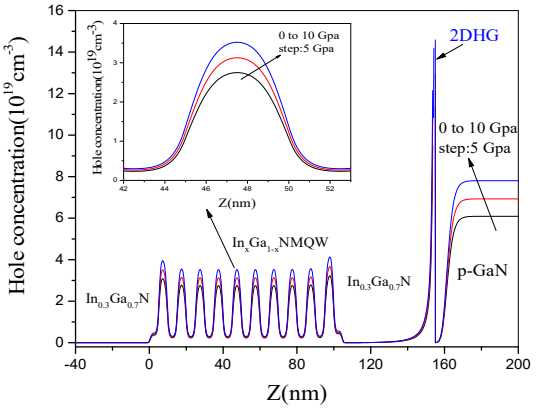

Figure 5. Hole concentration of InGaN/GaN MQW light-emitting diode as a function of the distance under different hydrostatic pressure.

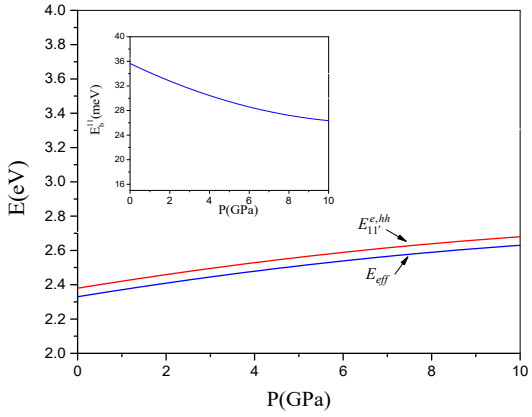

Figure 6. The first subband of transition energy $(E_{11'}^{e,hh})$ for the bound state of the heavy hole (hh), and effective band gap (E_{eff}) as a function of hydrostatic pressure at band edge $(k_{\square}=0)$ for InGaN/GaN MQW light-emitting diode. The inset represents the variation of the exciton binding energy of electron and hh as a function of the hydrostatic pressure.

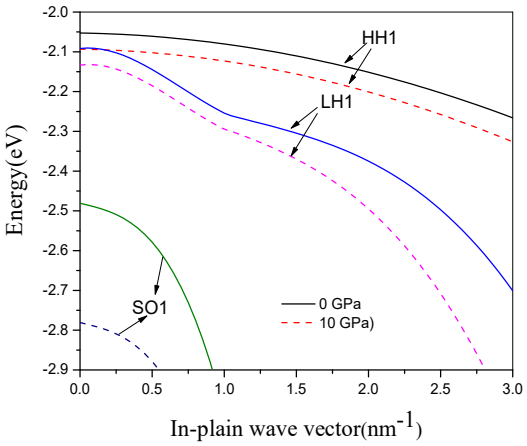

Figure 7. The valence band structure of heavy-hole (HH), Light-hole (LH), and split-off hole (SO) band InGaN/GaN quantum well is plotted along the k_x for hydrostatic pressure 0 Gpa (solid lines) and 10 GPa (dashed lines).

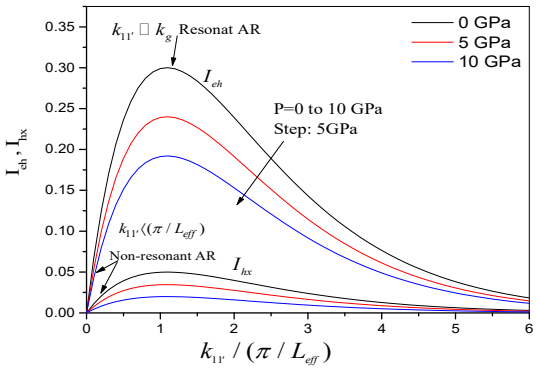

Figure 8. Overlap integrals versus transferred momentum $(k_{11'})$ for InGaN/GaN MQW light-emitting diode under different hydrostatic pressures.

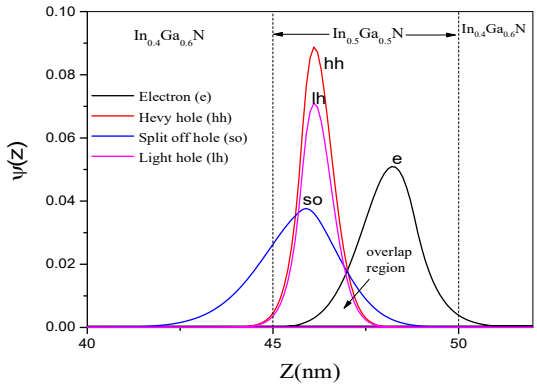

Figure 9. The first subband electron wave function ψ(z) versus the distance for InGaN/GaN MQW light-emitting diode under different hydrostatic pressures for the heavy hole (hh), light hole (lh), electron (e), and split-off band hole (so) with the quantum well in positions 45 to 50 nm.

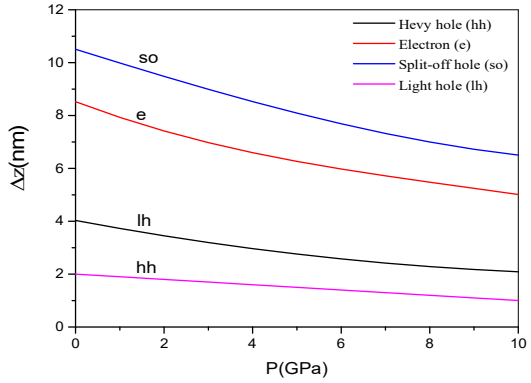

Figure 10. Carrier localization length for the first subband of the heavy hole (hh), light hole (lh), electron (e), and split-off band hole (so) in InGaN/GaN MQW light-emitting diode.

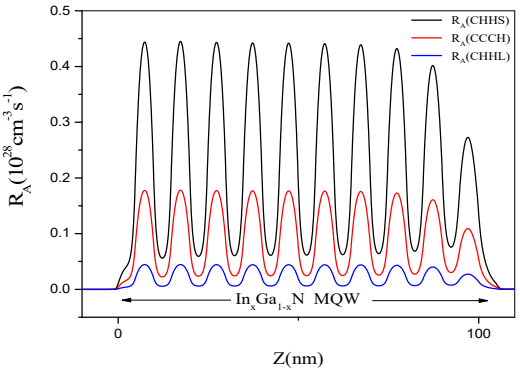

Figure 11. Auger recombination rate of CHHS, CCCH, CHHL, and total InGaN wells of MQW light-emitting diode as a function of the distance.

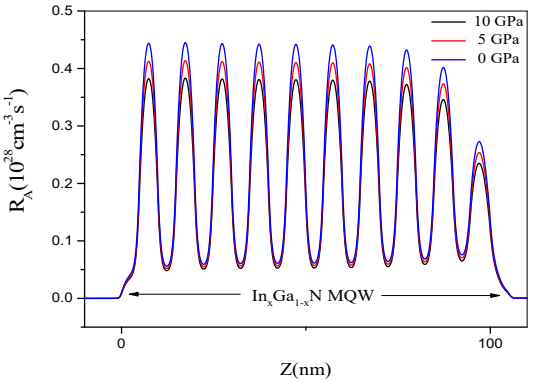

Figure 12. Auger recombination rate of InGaN/GaN MQW light-emitting diode as a function of the distance under different hydrostatic pressures.

4 Conclusions

Overall, this study examined the optical and electrical parameters of c-plane InGaN/GaN MQWLEDs under hydrostatic pressure. The results revealed that increasing the hydrostatic pressure in the range of 0-10 GPa could increase the amount of the carrier density up to $0.75\times10^{19} cm^{-3}$ and $0.56\times10^{19} cm^{-3}$ for holes and electrons, respectively, and the electric field rate up to $0.77 MV/cm$. On the other hand, this increase led to a reduction in the amount of the overlap integral of wave functions, excitonic binding energy, depth of the quantum well, and localized length of all carriers. Similarly, it decreased the Auger recombination down to $0.6\times10^{17} cm^{-3} s^{-1}$ in the multiple-quantum well regions, respectively. Our study findings provided further insight into the origin of the Auger current droop

under hydrostatic pressure in InGaN-based LEDs. Finally, the effective well width should be taken into account for a detailed examination of the Auger coefficient.

References

[1] A. David, N. G. Young, C. Lund, M. D. Craven, "Compensation between radiative and Auger recombinations in III-nitrides: The scaling law of separated-wavefunction recombinations." Appled Physics Letters, **115** (2019) 193502.

[2] C. K. Tan, W. Sun, J. J. WiererJr. N. Tansu, "Effect of interface roughness on Auger recombination in semiconductor quantum wells." AIP Advances, **7** (2017) 035212.

[3] D. Steiauf, E. Kioupakis, C. G. Van de Walle, "Auger Recombination in GaAs from First Principles." ACS Photonics, **1** (2014) 643.

[4] D. P. Han, C. H. Oh, D. G. Zheng, H. Kim, J. I. Shim, K. S. Kim, D. S. Shin, "Analysis of nonradiative recombination mechanisms and their impacts on the device performance of InGaN/GaN light-emitting diodes." Japanese Journal of Applied Physics, **54** (2015) 02BA01.

[5] W. Liu, C. Haller, Y. Chen, T. Weatherly, J. F. Carlin, G. Jacopin, R. Butté, and N. Grandjean, "Impact of defects on Auger recombination in c-plane InGaN/GaN single quantum well in the efficiency droop regime." Applied Physics Letters, **116** (2020) 222106.

[6] E. Kioupakis, P. Rinke, K. T. Delaney, C. G. Van de Walle, "Indirect Auger recombination as a cause of efficiency droop in nitride light-emitting diodes." Applied Physics Letters, **98** (2011) 161107.

[7] J. Piprek, "Efficiency droop in nitride-based light-emitting diodes." Physica Status Solidi A. **207** (2010) 2217.

[8] M. Auf der Maur, G. Moses, J. M. Gordon, X. Huang, Y. Zhao, E. A. Katz, "Temperature and intensity dependence of the open-circuit voltage of InGaN/GaN multi-quantum well solar cells." Solar Energy Materials and Solar Cells, **230** (2021) 111253.

[9] J. Piprek, F. Römer, B. Witzigmann, "On the uncertainty of the Auger recombination coefficient extracted from InGaN/GaN light-emitting diode efficiency droop measurements." Applied Physics Letters, **106** (2015) 101101.

[10] H. Y. Ryu, G. H. Ryu, C. Onwukaeme, B. Ma, "Temperature dependence of the Auger recombination coefficient in InGaN/GaN multiple-quantum-well light-emitting diodes." Optics Express, **28 (2020)** 27459.

[11] L. Cheng, Z. Li, J. Zhang, X. Lin, D. Yang, H. Chen, S. Wu, S. Yao, "Advantages of InGaN–GaN–InGaN Delta Barriers for InGaN-Based Laser Diodes." Nanomaterials, **11** (2021) 2070.

[12] S. Picozzi, R. Asahi, C. B. Geller, A. J. Freeman, "Accurate First-Principles Detailed-Balance Determination of Auger Recombination and Impact Ionization Rates in Semiconductors." Physical Review Letters, **89** (2002) 197601.

[13] A. S. Polkovnikov, G. G. Zegrya, "Auger recombination in semiconductor quantum wells." Physical Review B, **58** (1998) 4039.

[14] J. Piprek, Efficiency Models for GaN-Based Light-Emitting Diodes: Status and Challenges, Materials, **13**, 5174 (2020).

[15] J. M. McMahon, E. Kioupakis, S. Schulz, "Atomistic analysis of Auger recombination in *c*-plane (In,Ga)N/GaN quantum wells: Temperature-dependent competition between radiative and nonradiative recombination." Physical Review B, **105** (2022) 195307.

[16] H. Belmabrouk,, B. Chouchen , E. M. Feddi , F. Dujardin , I. Tlili , M. B. Ayed, M.Hichem Gazzah, "Modeling the simultaneous effects of thermal and polarization in InGaN/GaN based high electron mobility transistors." Optik, **207** (2020) 163883.

[17] X Huang et al., "Piezo-Phototronic Effect in a Quantum Well Structure." ACS Nano, **10** (2016) 5145.

[18] B. K. Ridley, W. J. Schaff, and L. F. Eastman, "Theoretical model for polarization superlattices: Energy levels and intersubband

transitions." Journal of Applied Physics, **94** (2003) 3972.

[19] O. Ambacher, J. Majewski, C. Miskys, et al., "Pyroelectric properties of Al (In) GaN/GaN hetero- and quantum well structures." Journal of Physics: Condensed Matter, **14** (2002) 3399.

[20] A. Asgari, K. Khalili, "Temperature dependence of InGaN/GaN multiple quantum well based high efficiency solar cell." Solar Energy Materials and Solar Cells, **95** (2011) 3124.

[21] V. Fiorentini, "Evidence for nonlinear macroscopic polarization in III–V nitride alloy heterostructures." Applied Physics Letters, 80 (2002) 1204.

[22] P. Perlin, L. Mattos, N. A. Shapiro, J. Kruger, W. S. Wong, T. Sands, Reduction of the energy gap pressure coefficient of GaN due to the constraining presence of the sapphire substrate, Journal of Applied Physics, **85** (1999) 2385.

[23] K. J. Bala, A. J. Peter, C. W. Lee, "Simultaneous effects of pressure and temperature on the optical transition energies in a $Ga_{0.7}In_{0.3}N$/GaN quantum ring." Chemical Physics, **495** (2017) 42.

[24] S. L. Chuang, C. S. Chang, "A band-structure model of strained quantum-well wurtzite semiconductors/" Semiconductor Science and Technology, **12** (1997) 252.

[25] S. L. Chuang and C. S. Chang, "k.p method for strained wurtzite semiconductors." Physical Review B, **54** (1996) 2491.

[26] J. Piprek and S. Nakamura, "Physics of high-power InGaN/GaN lasers." IEE Proceedings – Optoelectronics, **149** (2002) 145.

[27] R. Yahyazadeh, "Numerical Modeling of the Electronic and Electrical Characteristics of Multiple Quantum Well Solar Cells." Journal of Photonics Energy, **10** (2020) 045504.

[28] A. D. Andrew, E. O. O'Reilly, "Theoretical study of Auger recombination in a GaInNAs 1.3 μm quantum well laser structure." Applied Physics Letters, **84 (2004)** 182 (2004).

[29] J. Wang, P. V. Allmen, J. P. Leburton, K. J. Linden, "Auger Recombination in Long- Wavelength Strained-Layer Quantum-Well Structures." IEEE Journal of Quantum Electronics**, 31** (1995) 864.

[30] A. Asgari, M. Kalafi, L. Faraone, "A quasi-two-dimensional charge transport model of AlGaN/GaN high electron mobility transistors (HEMTs)." Physica E, **28** (2005) 491.

[31] W. W.-Ying, "Effects of interface roughness on photoluminescence full width at half maximum in GaN/AlGaN quantum wells." Chinese Physics B, **23** (2014) 117803.

[32] R. Yahyazadeh. "Effect of hydrostatic pressure on the radiative current density of InGaN/GaN multiple quantum well light emitting diodes." Optical and Quantum Electronics, **53** (2021) 571.

[33] R Yahyazadeh, Z Hashempour, "Numerical Modeling of Electronic and Electrical Characteristics of Al Ga N / GaN Multiple Quantum Well Solar Cells." Journal of Optoelectronical Nanostructures, **5** (2020) 81.

[34] S. H. Ha, S. L. Ban, "Binding energies of excitons in a strained wurtzite GaN/AlGaN quantum well influenced by screening and hydrostatic pressure." Journal of Physics: Condensed Matter, **20** (2008) 085218.

[35] J. G. Rojas-Briseno, I. Rodriguez-Vargas, M. E. Mora-Ramos, J. C. Martínez-Orozco, "Heavy and light exciton states in c-AlGaN/GaN asymmetric double quantum wells." Physica E. **124** (2020) 114248.

[36] P. Harrison and A Valavanis "Quantum Wells, Wires and Dots: Theoretical and Computational Physics of Semiconductor Nanostructures." 4th edn. (New York: John Wiley & Sons) (2016).

[37] E. Kasapoglu, H. Sari, N. Balkan, "Binding energy of excitons in symmetric and asymmetric coupled double quantum wells in a uniform magnetic field." Semiconductor Science and Technology, **15** (2000) 219.

[38] J. G. Rojas-Briseño, J. C. Martínez-Orozco, M. E.

Mora-Ramos, States of direct and indirect excitons in strained zinc-blende GaN/InGaN asymmetric quantum wells." Superlattices and Microstructures, **112** (2017) 574.

[39] D. Watson-Parris, M. J. Godfrey, P. Dawson, "Carrier localization mechanisms in $In_xGa_{1-x}N$/GaN quantum wells." Physical Review B, **83** (2011) 115321.

[40] B. Chouchen, M. H. Gazzah, A. Bajahzar, H. Belmabrouk, "Numerical modeling of InGaN/GaN p-i-n solar cells under temperature and hydrostatic pressure effects." AIP Advances, **9** (2019) 045313.

[41] B. Jogai, "Influence of surface states on the two-dimensional electron gas in AlGaN/GaN heterojunction field-effect transistors." Journal of Applied Physics, **93** (2003) 1631.

[42] B. Jogai, "Parasitic Hole Channels in AlGaN/GaN Heterojunction Structures." Physica Status Solidi (b), **233** (2002) 506.

[43] S. W. Corzine, L. Coldren, M. Mashanovitch, "Diode Lasers and Photonic Integrated Circuits" 2th edn. (New Jersey: John Wiley & Sons) (2012).

[44] G. P. Agrawal, N. K. Dutta, "Semiconductor Lasers." 2nd Edition. (New York: Springer) (1993).

[45] P. S. Zory, "Quantum well lasers" (Boston: Academic Press) 62 (1993).

[46] I. Vurgaftman, J. R Meyer, L. R. R Mohan, "Band parameters for III–V compound semiconductors and their alloys." Journal of Applied Physics, **89** (2001) 5815.

[47] S. Adachi, Physical Properties of III-V compounds. (New York: John Wiley & Sons (1992).

[48] V. B. Yekta, H. Kaatuzian, "Design considerations to improve high temperature characteristics of 1.3 μm AlGaInAs-InP uncooled multiple quantum well lasers: Strain in barriers." Optik, **122** (2011) 514.

[49] J. Hader; J. V. Moloney; S. W. Koch, "Microscopic evaluation of spontaneous emission- and Auger-processes in semiconductor lasers." IEEE Journal of Quantum Electronics, **41** (2005) 1217.

[50] I. H. Tan, G. L. Snider, L. D. Chang, E. L. Hu., "A self-consistent solution of Schrödinger–Poisson equations using a nonuniform mesh." Journal of Applied Physics, **68** (1990) 4071.

[51] S. L. Ruminates, M. S. Shur, "Material properties of nitrides summary." International Journal of High Speed Electronics and Systems, **14** (2004) 1.